# High photocatalytic activity of Fe2O3/TiO2 nanocomposites prepared by photodeposition for degradation of 2,4-dichlorophenoxyacetic acid_Beilstein Journal of Nanotechnology_2017, 8, 915

ORIGINALITY REPORT

| 16% | 7% | 14% | 3% |
|---|---|---|---|
| SIMILARITY INDEX | INTERNET SOURCES | PUBLICATIONS | STUDENT PAPERS |

PRIMARY SOURCES

| | | |
|---|---|---|
| 1 | Wai Ruu Siah, Hendrik O. Lintang, Leny Yuliati. "Role of lanthanum species in improving the photocatalytic activity of titanium dioxide", Catal. Sci. Technol., 2017<br>Publication | 2% |
| 2 | Lee, Shu Chin, Norhasnita Hasan, Hendrik O. Lintang, Mustaffa Shamsuddin, and Leny Yuliati. "Photocatalytic removal of 2,4-dichlorophenoxyacetic acid herbicide on copper oxide/titanium dioxide prepared by co-precipitation method", IOP Conference Series Materials Science and Engineering, 2016.<br>Publication | 2% |
| 3 | ori-oai.u-bordeaux1.fr<br>Internet Source | 1% |
| 4 | Roslan, Nur Azmina, Hendrik O. Lintang, and Leny Yuliati. "Enhanced Photocatalytic Performance of Copper-Modified Titanium | 1% |

# Digital Receipt

This receipt acknowledges that Turnitin received your paper. Below you will find the receipt information regarding your submission.

The first page of your submissions is displayed below.

| | |
|---|---|
| Submission author: | Leny Yuliati |
| Assignment title: | Workshop Plagiarisme UMC |
| Submission title: | High photocatalytic activity of Fe2O. |
| File name: | Beilstein_Journal_of_Nanotechnol... |
| File size: | 1.57M |
| Page count: | 12 |
| Word count: | 8,669 |
| Character count: | 44,405 |
| Submission date: | 17-Jan-2018 06:49PM (UTC+0700) |
| Submission ID: | 903552621 |

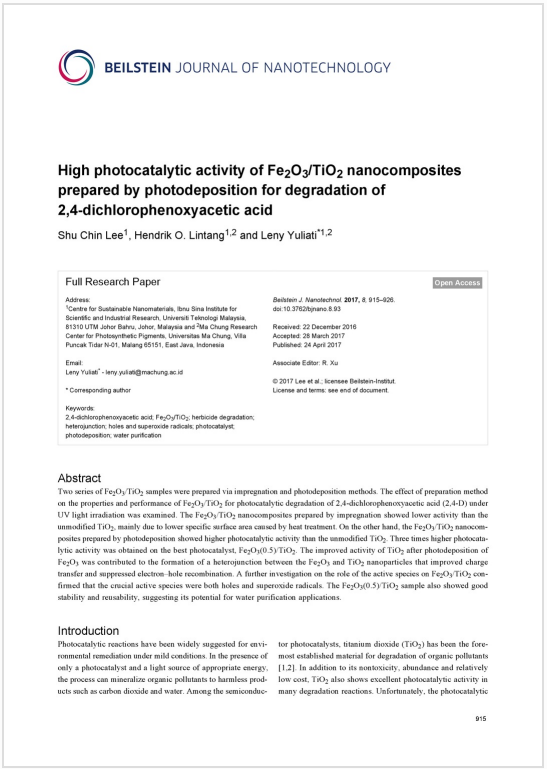

BEILSTEIN JOURNAL OF NANOTECHNOLOGY

**High photocatalytic activity of $Fe_2O_3/TiO_2$ nanocomposites prepared by photodeposition for degradation of 2,4-dichlorophenoxyacetic acid**

Shu Chin Lee[1], Hendrik O. Lintang[1,2] and Leny Yuliati*[1,2]

Full Research Paper — Open Access

Address:
[1]Centre for Sustainable Nanomaterials, Ibnu Sina Institute for Scientific and Industrial Research, Universiti Teknologi Malaysia, 81310 UTM Johor Bahru, Johor, Malaysia and [2]Ma Chung Research Center for Photosynthetic Pigments, Universitas Ma Chung, Villa Puncak Tidar N-01, Malang 65151, East Java, Indonesia

Email:
Leny Yuliati* - leny.yuliati@machung.ac.id

* Corresponding author

Keywords:
2,4-dichlorophenoxyacetic acid; $Fe_2O_3/TiO_2$; herbicide degradation; heterojunction; holes and superoxide radicals; photocatalyst; photodeposition; water purification

*Beilstein J. Nanotechnol.* **2017**, *8*, 915–926.
doi:10.3762/bjnano.8.93

Received: 22 December 2016
Accepted: 28 March 2017
Published: 24 April 2017

Associate Editor: R. Xu

© 2017 Lee et al.; licensee Beilstein-Institut.
License and terms: see end of document.

Abstract

Two series of $Fe_2O_3/TiO_2$ samples were prepared via impregnation and photodeposition methods. The effect of preparation method on the properties and performance of $Fe_2O_3/TiO_2$ for photocatalytic degradation of 2,4-dichlorophenoxyacetic acid (2,4-D) under UV light irradiation was examined. The $Fe_2O_3/TiO_2$ nanocomposites prepared by impregnation showed lower activity than the unmodified $TiO_2$, mainly due to lower specific surface area caused by heat treatment. On the other hand, the $Fe_2O_3/TiO_2$ nanocomposites prepared by photodeposition showed higher photocatalytic activity than the unmodified $TiO_2$. Three times higher photocatalytic activity was obtained on the best photocatalyst, $Fe_2O_3(0.5)/TiO_2$. The improved activity of $TiO_2$ after photodeposition of $Fe_2O_3$ was contributed to the formation of a heterojunction between the $Fe_2O_3$ and $TiO_2$ nanoparticles that improved charge transfer and suppressed electron–hole recombination. A further investigation on the role of the active species on $Fe_2O_3/TiO_2$ confirmed that the crucial active species were both holes and superoxide radicals. The $Fe_2O_3(0.5)/TiO_2$ sample also showed good stability and reusability, suggesting its potential for water purification applications.

Introduction

Photocatalytic reactions have been widely suggested for environmental remediation under mild conditions. In the presence of only a photocatalyst and a light source of appropriate energy, the process can mineralize organic pollutants to harmless products such as carbon dioxide and water. Among the semiconductor photocatalysts, titanium dioxide ($TiO_2$) has been the foremost established material for degradation of organic pollutants [1,2]. In addition to its nontoxicity, abundance and relatively low cost, $TiO_2$ also shows excellent photocatalytic activity in many degradation reactions. Unfortunately, the photocatalytic

915

# High photocatalytic activity of Fe2O3/TiO2 nanocomposites prepared by photodeposition for degradation of 2,4-dichlorophenoxyacetic acid_Beilstein Journal of Nanotechnology_2017, 8, 915

*by* Leny Yuliati

**Submission date:** 17-Jan-2018 06:49PM (UTC+0700)
**Submission ID:** 903552621
**File name:** Beilstein_Journal_of_Nanotechnology_2017,_8,_915.pdf (1.57M)
**Word count:** 8669
**Character count:** 44405

BEILSTEIN JOURNAL OF NANOTECHNOLOGY

# High photocatalytic activity of $Fe_2O_3/TiO_2$ nanocomposites prepared by photodeposition for degradation of 2,4-dichlorophenoxyacetic acid

Shu Chin Lee[1], Hendrik O. Lintang[1,2] and Leny Yuliati[*1,2]

Full Research Paper

Open Access

Address:
[1]Centre for Sustainable Nanomaterials, Ibnu Sina Institute for Scientific and Industrial Research, Universiti Teknologi Malaysia, 81310 UTM Johor Bahru, Johor, Malaysia and [2]Ma Chung Research Center for Photosynthetic Pigments, Universitas Ma Chung, Villa Puncak Tidar N-01, Malang 65151, East Java, Indonesia

Email:
Leny Yuliati* - leny.yuliati@machung.ac.id

* Corresponding author

Keywords:
2,4-dichlorophenoxyacetic acid; $Fe_2O_3/TiO_2$; herbicide degradation; heterojunction; holes and superoxide radicals; photocatalyst; photodeposition; water purification

*Beilstein J. Nanotechnol.* **2017,** *8,* 915–926.
doi:10.3762/bjnano.8.93

Received: 22 December 2016
Accepted: 28 March 2017
Published: 24 April 2017

Associate Editor: R. Xu



## Abstract

Two series of $Fe_2O_3/TiO_2$ samples were prepared via impregnation and photodeposition methods. The effect of preparation method on the properties and performance of $Fe_2O_3/TiO_2$ for photocatalytic degradation of 2,4-dichlorophenoxyacetic acid (2,4-D) under UV light irradiation was examined. The $Fe_2O_3/TiO_2$ nanocomposites prepared by impregnation showed lower activity than the unmodified $TiO_2$, mainly due to lower specific surface area caused by heat treatment. On the other hand, the $Fe_2O_3/TiO_2$ nanocomposites prepared by photodeposition showed higher photocatalytic activity than the unmodified $TiO_2$. Three times higher photocatalytic activity was obtained on the best photocatalyst, $Fe_2O_3(0.5)/TiO_2$. The improved activity of $TiO_2$ after photodeposition of $Fe_2O_3$ was contributed to the formation of a heterojunction between the $Fe_2O_3$ and $TiO_2$ nanoparticles that improved charge transfer and suppressed electron–hole recombination. A further investigation on the role of the active species on $Fe_2O_3/TiO_2$ confirmed that the crucial active species were both holes and superoxide radicals. The $Fe_2O_3(0.5)/TiO_2$ sample also showed good stability and reusability, suggesting its potential for water purification applications.

## Introduction

Photocatalytic reactions have been widely suggested for environmental remediation under mild conditions. In the presence of only a photocatalyst and a light source of appropriate energy, the process can mineralize organic pollutants to harmless products such as carbon dioxide and water. Among the semiconductor photocatalysts, titanium dioxide ($TiO_2$) has been the foremost established material for degradation of organic pollutants [1,2]. In addition to its nontoxicity, abundance and relatively low cost, $TiO_2$ also shows excellent photocatalytic activity in many degradation reactions. Unfortunately, the photocatalytic

performance of $TiO_2$ is generally restricted by its high charge carrier recombination rate. Therefore, the modification of $TiO_2$ in order to reduce such recombinations remains a critical task. Another important point is the emphasis on using an environmentally safe and sustainable material as the modifier.

As one of the best modifiers, the use of a co-catalyst has been recognized to improve the photocatalytic performance of semiconductor photocatalysts as it promotes charge separation and suppresses photocorrosion of the semiconductor photocatalyst [3,4]. One of the potential co-catalyst modifiers is iron(III) oxide ($Fe_2O_3$), which is nontoxic, stable, cost effective and found abundantly in the earth. It has been reported that $Fe_2O_3$ can be used to increase the photocatalytic activity or selectivity of semiconductor photocatalysts for degradation of organic pollutants [5-15]. Commonly, the reported methods for the preparation of $Fe_2O_3/TiO_2$ include impregnation [5,6,16-18], sol–gel [7,19], and hydrothermal methods [8-10]. A combination of several processes has also been employed, such as the electrospinning method combined with a hydrothermal approach [11], plasma enhanced-chemical vapor deposition (PECVD) and radio frequency (RF) sputtering approach [12], and plasma enhanced-chemical vapor deposition and atomic layer deposition (ALD) followed by thermal treatment [13]. Among these preparation methods, impregnation is a commonly used approach for the preparation of $Fe_2O_3/TiO_2$ as it offers a simple process. However, there are contradicting reports on the performance of $Fe_2O_3/TiO_2$ catalysts prepared by the impregnation method. While some groups reported good photocatalytic activity [5,6], others showed contrasting results [16-18], which have resulted in different opinions regarding the contribution of the $Fe_2O_3$. Since the impregnation method usually involves heat treatment, the properties of $TiO_2$ such as the ratio of anatase/rutile, particle size, as well as specific surface area may be altered during this process and could influence the photocatalytic activity of $TiO_2$ [16,17]. Therefore, careful considerations shall be taken before concluding whether the $Fe_2O_3$ is beneficial or not in regards to improving the photocatalytic activity of $TiO_2$.

Another simple method to produce $Fe_2O_3/TiO_2$ is a mechanochemical milling approach that can be carried out at ambient conditions [14]. Even though high activity was obtained, evidence of the formation of good contact between $Fe_2O_3$ and $TiO_2$ nanoparticles was not provided. Recently, the photodeposition method has been proposed as a suitable method to directly investigate the role of added copper or lanthanum species without such heat-treatment effects [20,21]. Moreover, the modification of $TiO_2$ nanoparticles by photodeposition resulted in an improved photocatalytic activity as compared to unmodified $TiO_2$ [20-22]. Therefore, it is meaningful to employ the photodeposition method to prepare $Fe_2O_3/TiO_2$ catalysts without heat treatment at ambient conditions. Using iron(III) nitrate nonahydrate as the precursor, active and stable $Fe_2O_3/TiO_2$ was successfully prepared via photodeposition [15]. However, the actual amount of iron precursor in the prepared $Fe_2O_3/TiO_2$ was much lower than that added. In the present study, $Fe_2O_3/TiO_2$ nanocomposites were prepared by a similar approach but using iron(III) acetylacetonate as the precursor to facilitate a complete photodeposition process. The properties and activity results were compared with those prepared by the commonly used impregnation approach. Furthermore, to the best of our knowledge, there is no study on the activity comparison between $Fe_2O_3/TiO_2$ prepared by the widely used impregnation and the photodeposition methods, which is important to determine the optimal method for the preparation of photocatalyst materials with good properties.

In this study, both impregnation and photodeposition methods were used to modify $TiO_2$ nanoparticles with $Fe_2O_3$ in order to investigate the effect of preparation method on the properties and photocatalytic activity of the nanocomposites with respect to the degradation of 2,4-dichlorophenoxyacetic acid (2,4-D) under irradiation of UV light. 2,4-D is a herbicide widely utilized in the agricultural industry; it can be found in water sources due to its common use in controlling broadleaf weeds [23]. Excessive exposure of 2,4-D leads to adverse impacts on the ecosystem, and thus, the toxic organic pollutant must be eliminated from the water source utilizing efficient approaches. Various removal methods of 2,4-D have been developed, including adsorption [24], biodegradation [25], ozonation [26], and photocatalytic degradation [15,20-22,27-32], of which the latter has been recognized for its capability to decompose the organic pollutant under a mild environment. In the present work, it was shown that the different preparation methods resulted in distinctly different properties and photocatalytic activity. Better properties and the improved activity of $Fe_2O_3/TiO_2$ nanocomposites prepared by photodeposition for the degradation of 2,4-D were discussed. In addition to identifying the charge transfer capability of the $Fe_2O_3/TiO_2$ catalyst for improved photocatalytic activity, the role of the active species on the $Fe_2O_3/TiO_2$ nanocomposites prepared by the photodeposition method was further investigated in order to understand the important active species contributing to the photocatalytic activity.

## Results and Discussion

### Photocatalytic activity comparison

The photocatalytic efficiency of the $Fe_2O_3/TiO_2$ nanocomposites prepared by impregnation was evaluated for the removal of 2,4-D under UV light illumination at room temperature for 1 h. Under the same conditions, it was confirmed that no photolysis

of 2,4-D was obtained without photocatalyst. After adsorption–desorption equilibrium was achieved in 1 h, adsorption experiments were conducted in the absence of light for another 1 h. Related to the following sample descriptions, NT represents no treatment, IM indicates the samples were prepared by impregnation, PD indicates samples were prepared by photodeposition, and T indicates an additional heat treatment was carried out. Figure 1A demonstrates that the $TiO_2$ (NT) sample gave 30% adsorption of 2,4-D. After heat treatment at 500 °C, the adsorption of 2,4-D on the samples was greatly suppressed. All the $TiO_2$ (IM_T) and $Fe_2O_3/TiO_2$ (IM) nanocomposites showed 2,4-D adsorption of 2–3%. The photocatalytic activity of the photocatalysts was each determined by exclusion of 2,4-D adsorption and the results are shown in Figure 1B. There was no significant difference observed between the $TiO_2$ (NT) and the $TiO_2$ (IM_T), which showed 2,4-D removal of 78 and 76%, respectively. Introducing various amounts of $Fe_2O_3$ on the $TiO_2$ material via impregnation did not improve the photocatalytic activity of the $TiO_2$. With increased loading of $Fe_2O_3$, the photocatalytic performance of $TiO_2$ in fact decreased. As another control experiment, α-$Fe_2O_3$ synthesized at 500 °C for 4 h was also tested for the removal of 2,4-D. The removal of 2,4-D using α-$Fe_2O_3$ was only 2% after 1 h of UV illumination, which might be due to the fast charge recombination in hematite [13,15,33].

In contrast to the samples synthesized by the impregnation method, the high adsorption of 2,4-D at 25–30% was still achieved on the photodeposition synthesized samples as shown in Figure 2A. Only a slight decrease in adsorption was obtained with increasing Fe/Ti ratio, suggesting that the adsorption sites were not covered by the deposition of $Fe_2O_3$. Figure 2B shows the photocatalytic performance of the $TiO_2$ and the $Fe_2O_3/TiO_2$ (PD) nanocomposites after the exclusion of the 2,4-D adsorption. No significant difference in the activity was obtained for the $TiO_2$ (NT) and the $TiO_2$ (PD_T), which showed 2,4-D removal of 78 and 76%, respectively. This result clearly demonstrated that, in contrast to the heat treatment, the photodeposition treatment did not alter the photocatalytic performance of $TiO_2$. It is worth noting that after the Fe species were photodeposited on the $TiO_2$, all the nanocomposites gave superior activity as compared to that of unmodified $TiO_2$. The Fe/Ti ratio of 0.5 mol % was found to be the optimum loading in which the

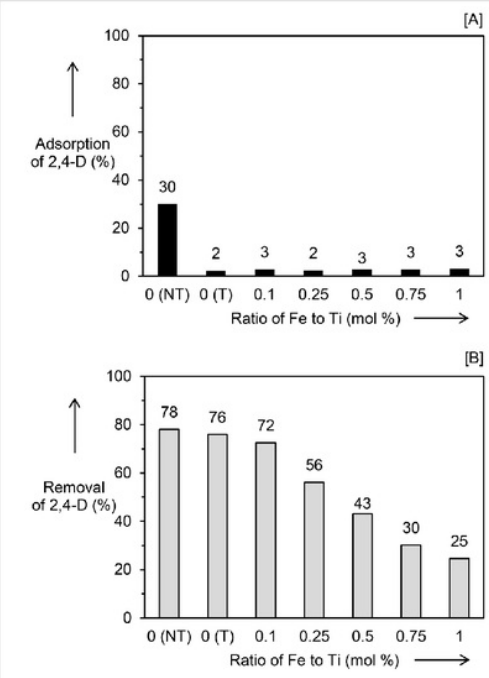


**Figure 1:** (A) Adsorption and (B) photocatalytic removal of 2,4-D using $TiO_2$ (NT), $TiO_2$ (IM_T) and series of $Fe_2O_3/TiO_2$(IM). NT represents no treatment, IM shows the samples were prepared by impregnation method, and T indicates an additional heat treatment was carried out on the sample.

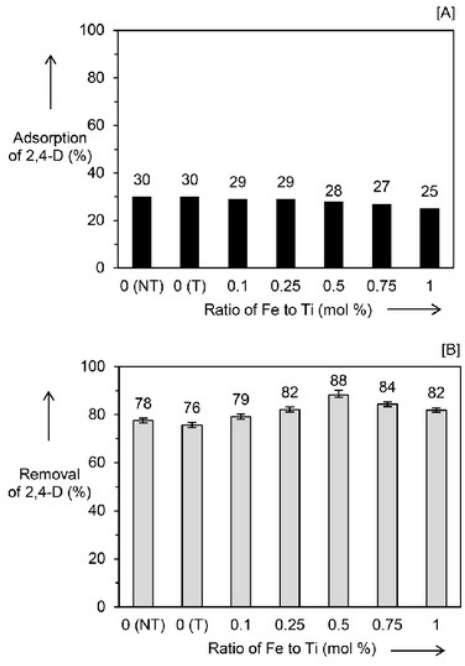


**Figure 2:** (A) Adsorption and (B) photocatalytic removal of 2,4-D over $TiO_2$ (NT), $TiO_2$ (PD_T) and a series of $Fe_2O_3/TiO_2$(PD) samples. Error bars in (B) are shown for comparison purposes. NT represents no treatment, PD shows the samples were prepared by photodeposition method, and T indicates an additional photodeposition treatment was carried out on the sample.

$Fe_2O_3$(0.5)/$TiO_2$ (PD) sample showed the highest removal of 88% after 1 h irradiation. These results showed that different synthesis methods lead to different photocatalytic performance. The photocatalysts prepared by photodeposition showed superior performance compared to those prepared by the impregnation method.

## Properties comparison

The structural, optical, and physical properties of the $Fe_2O_3$/$TiO_2$ photocatalysts synthesized by impregnation and photodeposition were investigated and compared to clarify the characteristic differences of the photocatalysts obtained from the different preparation methods. X-ray diffraction (XRD) patterns were collected for the $Fe_2O_3$/$TiO_2$ (IM) series prepared by the impregnation method. $TiO_2$ (NT) exhibited diffraction peaks corresponding to the anatase phase (JCPDS file No. 21-1272), which were observed at 2θ of 25.35, 38.10, 48.05, 54.55, and 62.60°, corresponding to (101), (004), (200), (105), and (204) diffraction planes, respectively (see Supporting Information File 1, Figure S1). After heat treatment, the $TiO_2$ (IM_T) sample showed improved crystallinity without any changes in the structural phase, which was found to be pure anatase. After addition of Fe species, the crystallinity of the $Fe_2O_3$/$TiO_2$ (IM) nanocomposites did not change and was confirmed to be similar to that of the $TiO_2$ (IM_T) sample. The characteristic diffraction peaks corresponding to the anatase phase of $TiO_2$ remained in all samples without any peak shifting. Furthermore, the existence of new diffraction peaks of α-$Fe_2O_3$ (JCPDS file No. 33-0664) was not identified, suggesting that the low loading of $Fe_2O_3$ might be dispersed well on the surface of the $TiO_2$.

The Scherrer equation was used to calculate the crystallite size of the samples based on the (101) peak at 2θ of 25.35°. As listed in Table 1, the crystallite size of the $TiO_2$ (NT) was initially 9.3 nm (Table 1, entry 1). After heat treatment, the crystallite size of $TiO_2$ (IM_T) increased to 14.3 nm (Table 1, entry 2). The addition of $Fe_2O_3$ did not further influence the crystallite size. All the $Fe_2O_3$/$TiO_2$ (IM) nanocomposites had a crystallite size in a range of 14.3–15.9 nm (Table 1, entries 3–7), which was close to that of the $TiO_2$ (IM_T). Since there was no much difference in the crystallinity and crystallite size between the $TiO_2$ (IM_T) and $Fe_2O_3$/$TiO_2$ (IM), it was suggested that the improved crystallinity and crystallite size as compared to $TiO_2$ (NT) was mostly due to the heat treatment only and not to the addition of $Fe_2O_3$.

The XRD patterns of the $Fe_2O_3$/$TiO_2$ (PD) series that was synthesized by the photodeposition method were also recorded (see Supporting Information File 1, Figure S2). Different from the case of heat treatment with the impregnation method, the photodeposition treatment did not change the crystallinity of both the $TiO_2$ (PD_T) and the $Fe_2O_3$/$TiO_2$ (PD) nanocomposites. No peak shifting and the appearance of no new diffraction peak suggested good dispersion of the Fe species on the surface of the $TiO_2$. The crystallite size of the $Fe_2O_3$/$TiO_2$ (PD) is given in Table 1. All samples have a crystallite size in the range of 8.8–9.3 nm (Table 1, entries 8–13), suggesting that the crystallite size was not altered by the photodeposition method. Comparing the two synthesis methods, it was obvious that the photodeposition method maintained both crystallinity and crystallite size of the $TiO_2$, while the impregnation method led to higher crystallinity and crystallite size. This difference was caused by the different preparation conditions; the photodeposition was conducted under mild synthesis conditions under illumination of UV light at room temperature, whereas a high heating temperature of 500 °C was used during the impregnation method.

**Table 1:** Crystallite size and band gap energy ($E_g$) of the unmodified $TiO_2$ and $Fe_2O_3$/$TiO_2$nanocomposites prepared by impregnation (IM) and photodeposition (PD) methods. NT represents no treatment and T indicates an additional heat treatment was carried out on the sample.

| Entry | Samples | Crystallite size (nm)[a] | $E_g$ (eV)[b] |
|---|---|---|---|
| 1 | $TiO_2$ (NT) | 9.3 | 3.30 |
| 2 | $TiO_2$ (IM_T) | 14.3 | 3.29 |
| 3 | $Fe_2O_3$(0.1)/$TiO_2$ (IM) | 14.3 | 3.29 |
| 4 | $Fe_2O_3$(0.25)/$TiO_2$ (IM) | 15.9 | 3.27 |
| 5 | $Fe_2O_3$(0.5)/$TiO_2$ (IM) | 15.8 | 3.27 |
| 6 | $Fe_2O_3$(0.75)/$TiO_2$ (IM) | 15.8 | 3.26 |
| 7 | $Fe_2O_3$(1)/$TiO_2$ (IM) | 15.8 | 3.25 |
| 8 | $TiO_2$ (PD_T) | 8.8 | 3.29 |
| 9 | $Fe_2O_3$(0.1)/$TiO_2$ (PD) | 9.3 | 3.28 |
| 10 | $Fe_2O_3$(0.25)/$TiO_2$ (PD) | 8.8 | 3.27 |
| 11 | $Fe_2O_3$(0.5)/$TiO_2$ (PD) | 8.8 | 3.27 |
| 12 | $Fe_2O_3$(0.75)/$TiO_2$ (PD) | 8.8 | 3.25 |
| 13 | $Fe_2O_3$(1)/$TiO_2$ (PD) | 9.3 | 3.24 |

[a]Scherrer equation was used to calculate the crystallite size.
[b]Tauc plot was used to determine the $E_g$.

The optical absorption properties of the nanocomposites prepared by the impregnation method were investigated (see Supporting Information File 1, Figure S3). The $TiO_2$ (NT) sample absorbs light in the UV region and exhibits a characteristic band for $TiO_2$ at about 370 nm due to the charge transfer of $O^{2-} \rightarrow Ti^{4+}$ and electron excitation from the valence band (VB) to the conduction band (CB) [20,21]. Both the heat treatment and addition of Fe species did not affect the light absorption of the $TiO_2$ (NT) in the UV and visible region. Owing to the low loading of Fe, there was no additional absorption peak corre-

sponding to the Fe species. The bandgap energy ($E_g$) of the unmodified $TiO_2$ and the nanocomposites were studied by a Tauc plot, considering the indirect transition in anatase $TiO_2$ [34]. The Tauc plot of the $TiO_2$ (NT) and the $Fe_2O_3/TiO_2$ (IM) nanocomposites was derived by plotting $(\alpha h\nu)^{1/2}$ versus $h\nu$. The $E_g$ value was obtained from the $x$-intercept using the linear extrapolation in the plot. Table 1 summarizes the $E_g$ values of the samples. The $TiO_2$ (NT) sample has an $E_g$ of 3.30 eV (Table 1, entry 1). The heat-treated $TiO_2$ (IM_T) showed an $E_g$ value of 2.29 eV (Table 1, entry 2), close to the value of the $TiO_2$ (NT), indicating that a high calcination temperature of 500 °C did not affect the optical properties of the $TiO_2$. The addition of Fe species did not result in significant changes to the $E_g$ of the $TiO_2$, which with an increasing Fe/Ti ratio from 0.1 to 1 mol % only slightly reduced the $E_g$ from 3.29 to 3.25 eV (Table 1, entries 3–7). The insignificant change in the $E_g$ suggested that the Fe species might be loaded on the surface instead of incorporated into the $TiO_2$ lattice. The obtained results matched well with the nanocomposite prepared via adsorption and decomposition of the Fe(III) complex at 400 °C [5]. This is in contrast to the one prepared by the sol–gel method that showed an obviously reduced $E_g$ value as the Fe ions were incorporated into the $TiO_2$ lattice [7,19].

Diffuse reflectance (DR) UV–vis spectra and Tauc plots of the nanocomposites prepared by the photodeposition method were also measured (see Supporting Information File 1, Figure S4). Similar to the nanocomposites prepared by the impregnation method, the photodeposition treatment and addition of Fe species also did not much affect the light absorption or the $E_g$ of both the $TiO_2$ (PD_T) and $Fe_2O_3/TiO_2$ (PD) sample. Besides, the slightly decreased $E_g$ from 3.28 to 3.24 eV (Table 1, entries 9–13) also suggested that Fe species might be loaded on the surface of the $TiO_2$ via photodeposition.

The amount of Fe content loaded on the $Fe_2O_3/TiO_2$ nanocomposites was determined by the inductively coupled plasma optical emission spectrometer (ICP-OES) measurement, as listed in Table 2. The Fe/Ti composition (mol %) obtained from the measurement confirmed that the Fe content loaded on the $TiO_2$ was close to the nominal added amount. These results clearly suggested that in the given range of Fe loading (0.1–1 mol %), all the iron precursor was successfully photodeposited onto the $TiO_2$.

The Brunauer–Emmett–Teller (BET) specific surface area of the $TiO_2$ and the $Fe_2O_3/TiO_2$ nanocomposites prepared by the impregnation and the photodeposition method are shown in Figure 3. The $TiO_2$ (NT) has a large specific surface area of 298 $m^2/g$. After calcination at 500 °C, the specific surface area of the $TiO_2$ (IM_T) dropped drastically to 80 $m^2/g$. The addition of $Fe_2O_3$ to $TiO_2$ via the impregnation method did not significantly change the specific surface area of the $TiO_2$ (IM_T), given that all nanocomposites have values in the range of 72–80 $m^2/g$. This result obviously showed that it was the heat treatment and not the $Fe_2O_3$ addition that caused the decrease in the BET specific surface area.

In contrast to the nanocomposites prepared by the impregnation method, only a slight gradual decrease was observed with increasing Fe/Ti ratio in the $Fe_2O_3/TiO_2$ nanocomposites prepared from the photodeposition method. The nanocomposite sample with the lowest Fe/Ti ratio of 0.1 mol % still showed a large surface area of 297 $m^2/g$, while the nanocomposite sample with the highest Fe/Ti ratio of 1 mol % showed a value of 265 $m^2/g$. These results again confirmed that the mild photodeposition method did not influence the properties of the $TiO_2$ (NT).

As shown in Figure 1 and Figure 2, nanocomposites synthesized by the photodeposition method exhibited superior adsorp-

**Table 2:** The composition of the $Fe_2O_3/TiO_2$ (PD) nanocomposites (ratio of Fe/Ti (mol %)) determined from ICP-OES measurements. PD indicates samples that were prepared with the photodeposition method.

| Samples | Fe/Ti (mol %) |
|---|---|
| $Fe_2O_3(0.1)/TiO_2$ (PD) | 0.11 |
| $Fe_2O_3(0.25)/TiO_2$ (PD) | 0.20 |
| $Fe_2O_3(0.5)/TiO_2$ (PD) | 0.45 |
| $Fe_2O_3(0.75)/TiO_2$ (PD) | 0.72 |
| $Fe_2O_3(1)/TiO_2$ (PD) | 1.02 |

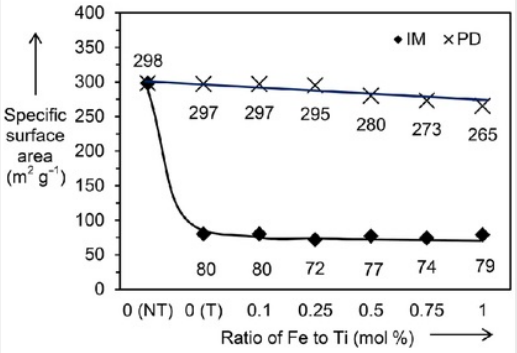


**Figure 3:** BET specific surface area of $TiO_2$ (NT), $TiO_2$ (T) and the series of $Fe_2O_3/TiO_2$ samples prepared by both impregnation (IM) and photodeposition (PD). NT represents no treatment and T indicates an additional heat treatment or photodeposition treatment was carried out on the sample.

tion and photocatalytic activity than those synthesized by the impregnation method. The higher percentage of 2,4-D adsorption could result from the larger BET specific surface area of the samples prepared by the photodeposition method. As for the photocatalytic activity, a few important parameters have been reported to contribute to a high photocatalytic activity, including high crystallinity [35], small crystallite size [36], and high specific surface area [30,36]. Generally, materials with high crystallinity have fewer crystal defects, while a smaller crystallite size decreases the diffusion path length between the charge carriers – these two parameters can suppress recombination of photogenerated electrons–holes. On the other hand, materials with a large specific surface area have many available surface active sites for reaction to take place, which can lead to high photocatalytic activity. In the case of nanocomposites prepared by the impregnation method, even though improved crystallinity was observed, it might be compensated by the larger crystallite size and a lower specific surface area, which overall led to decreased photocatalytic activity. Since the photodeposition method did not have a great influence on the crystallinity, crystallite size, and the BET specific surface area, the effects caused by such changes can be avoided, and the main factors contributing to the photocatalytic activity can be narrowed down solely to the added Fe species.

## Improved properties

Since nanocomposites synthesized by the photodeposition method showed better photocatalytic activity than the nanocomposites synthesized by the impregnation method, further detailed investigations were carried out on nanocomposites synthesized by the photodeposition method. Transmission electron microscopy (TEM) and high-resolution TEM (HRTEM) images of both unmodified $TiO_2$ (NT) and $Fe_2O_3(0.5)/TiO_2$ (PD) are shown in Figure 4. As shown in Figure 4a, the $TiO_2$ (NT) sample has spherical particles with a diameter of 7–9 nm. This result agreed well with the crystallite size calculated by the Scherrer equation previously discussed. The HRTEM image of the $TiO_2$ (NT) sample displayed in Figure 4b shows a lattice fringe spacing of 0.35 nm attributed to the anatase $TiO_2$(101) crystal plane. Figure 4d shows a HRTEM image of $Fe_2O_3(0.5)/TiO_2$ (PD). It was evident that the deposition of Fe did not change the morphology of the $TiO_2$. Since the lattice fringe spacing of 0.27 nm related to the $Fe_2O_3$(104) crystal plane was observed, the possible formation of a heterojunction between $Fe_2O_3$ and $TiO_2$ was considered. Such close contact would cause the carrier diffusion length to be short, and in turn, would improve the charge transfer. This would thus suppress charge recombination, which is crucial to enhance the photocatalytic activity.

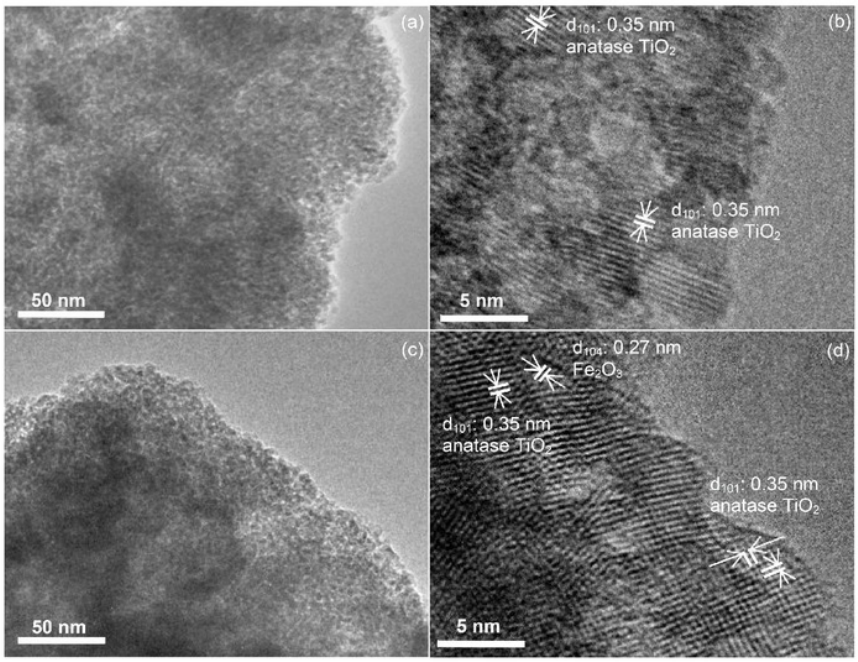


**Figure 4:** (a) TEM image of unmodified $TiO_2$ (NT) and (b) its respective HRTEM image, (c) TEM image of $Fe_2O_3(0.5)/TiO_2$ (PD) and (d) its respective HRTEM image.

The formation of $Fe_2O_3$ was in good agreement with other reported photodeposition methods when using a different iron precursor, Fe(III) nitrate nonahydrate [15]. Due to the oxidative condition during the synthesis process, the Fe(III) acetylacetonate precursor could be decomposed to $Fe_2O_3$ such as by the photogenerated oxygen radicals [21]. It was demonstrated that the use of the Fe(III) acetylacetonate precursor led to a complete photodeposition to form $Fe_2O_3$, as also supported by ICP-OES results discussed above.

The improved charge transfer of the $Fe_2O_3(0.5)/TiO_2$ (PD) sample was further clarified using electrochemical impedance spectroscopy (EIS). Figure 5 shows the Nyquist plots of the unmodified $TiO_2$ (NT) and $Fe_2O_3(0.5)/TiO_2$ (PD) samples. The arc radius of the Nyquist plot reflects the impedance of the interface layer arising at the electrode surface. The smaller the arc radius the better the charge transfer [37]. It is worth noting here that the $Fe_2O_3(0.5)/TiO_2$ (PD) material has a smaller arc radius than unmodified $TiO_2$. These results clearly suggest that the $Fe_2O_3(0.5)/TiO_2$ (PD) material has a lower impedance than unmodified $TiO_2$, indicating enhanced conductivity of $TiO_2$ after photodeposition of $Fe_2O_3$. The electron transfer kinetics of a material can be calculated using Equation 1:

$$k = \frac{RT}{n^2F^2AR_{ct}C^\circ} \quad (1)$$

where $k$ is the heterogeneous electron-transfer rate constant, $R$ is the gas constant, $T$ is temperature (K), $n$ represents the number of transferred electrons per molecule of the redox probe, $F$ is the Faraday constant, $A$ is the electrode area ($cm^2$), $R_{ct}$ is the charge transfer resistance that can be obtained from the fitted Nyquist plot, and $C^\circ$ is the concentration of the redox couple in the bulk solution (ferricyanide/ferrocyanide) [38].

From the fitted impedance data shown in Figure 5, the $Fe_2O_3(0.5)/TiO_2$ (PD) material gave an $R_{ct}$ value of 2.87 kΩ, which was smaller than that of unmodified $TiO_2$ (NT) with $R_{ct}$ = 3.40 kΩ. The lower $R_{ct}$ value obviously suggested that the $Fe_2O_3(0.5)/TiO_2$ (PD) material has better charge conductivity and transfer capability than unmodified $TiO_2$ (NT). Furthermore, the $k$ values of the $Fe_2O_3(0.5)/TiO_2$ (PD) sample and unmodified $TiO_2$ (NT) were calculated to be $2.96 \times 10^{-4}$ and $2.49 \times 10^{-4}$ cm/s, respectively, indicating that the charge transfer that on the $Fe_2O_3(0.5)/TiO_2$ (PD) sample proceeded faster than on unmodified $TiO_2$. As suggested from the HRTEM result, the formation of an $Fe_2O_3/TiO_2$ heterojunction might promote better electron transfer which resulted in improved photocatalytic activity of the $Fe_2O_3(0.5)/TiO_2$ (PD) material.

Photoluminescence has been associated with electron–hole recombination of a photocatalyst [39]. In this study, the ability of an $Fe_2O_3$ co-catalyst to accept photogenerated electrons as well as to suppress the recombination of electron–holes on the $TiO_2$ was supported by the fluorescence spectroscopy results. The emission spectra of the unmodified $TiO_2$ (NT) and the $Fe_2O_3(0.5)/TiO_2$ (PD) samples under a fixed excitation wavelength of 218 nm are shown in Figure 6. $TiO_2$ exhibited three emission peaks at 407, 466 and 562 nm. The emission at 407 nm could be caused by the radiative recombination of self-trapped excitons, while peaks at 466 and 562 nm were attributed to the charge transfer of an oxygen vacancy trapped electron. The obtained results agreed well with the reported literature [39]. The $Fe_2O_3(0.5)/TiO_2$ (PD) material showed a decreased emission intensity as compared to the unmodified $TiO_2$ (NT), suggesting that the photogenerated electrons on $TiO_2$ could be transferred and trapped by $Fe_2O_3$. This resulted in a suppression of the electrons–hole recombination on $TiO_2$, which led to the improved removal of 2,4-D.

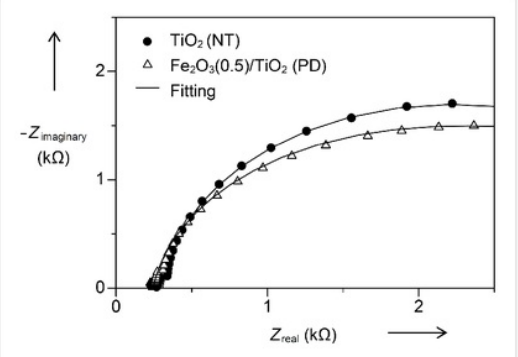


**Figure 5:** Nyquist plots of unmodified $TiO_2$ (NT) and $Fe_2O_3(0.5)/TiO_2$ (PD) with the respective model fitting.

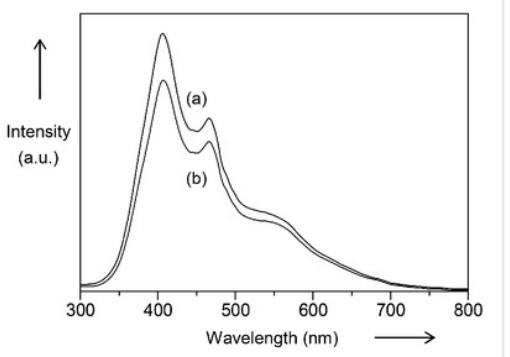


**Figure 6:** Emission spectra of (a) unmodified $TiO_2$ (NT) and (b) $Fe_2O_3(0.5)/TiO_2$ (PD).

For comparison, a Nyquist plot and emission spectrum of the $Fe_2O_3(0.1)/TiO_2$ (IM) material were also measured and given in Supporting Information File 1, Figures S5 and S6, respectively. It was clear that the $Fe_2O_3(0.1)/TiO_2$ (IM) had a smaller arc radius of the Nyquist plot and slightly lower emission intensity than the $TiO_2$ (NT), suggesting that the $Fe_2O_3(0.1)/TiO_2$ (IM) has better charge transfer and suppressed electron–hole recombination. Unfortunately, these better properties did not promote the photocatalytic activity of the $Fe_2O_3(0.1)/TiO_2$ (IM). It turns out that the photocatalytic activity of $Fe_2O_3(0.1)/TiO_2$ (IM) would be more influenced by the distinct decrease in the specific surface area, as discussed previously.

## Active species and stability

It has been reported that the reaction pathways for photocatalytic oxidation of organic pollutants are dominated by several active species, such as holes, superoxide radicals, and hydroxyl radicals [39]. Among the scavengers of active species, ammonium oxalate has been reported as an efficient hole scavenger [40], benzoquinone acts to scavenge superoxide radicals efficiently [40], while *tert*-butanol has fast reaction with hydroxyl radicals [27,40] and hence, they were selected for the scavenger studies. As shown in Figure 7, the photocatalytic reactions under 1 h of UV illumination were evaluated in the presence of each scavenger on the unmodified $TiO_2$ (NT) and the $Fe_2O_3(0.5)/TiO_2$ (PD). For the reaction conducted on the unmodified $TiO_2$ (NT), the addition of ammonium oxalate was found to drastically suppress the activity, which was reduced from 78 to 13%, equivalent to 5.8 times lower than the one without scavenger. The inhibited activity indicated the importance of the photogenerated holes for the oxidation of 2,4-D. When benzoquinone was added, the activity was reduced from 78 to 66%, suggesting that superoxide radicals also played a role in the oxidation process of 2,4-D. In contrast, addition of *tert*-butanol did not affect the activity of the $TiO_2$ (NT), indicating that hydroxyl radicals are not the important active species for the reaction.

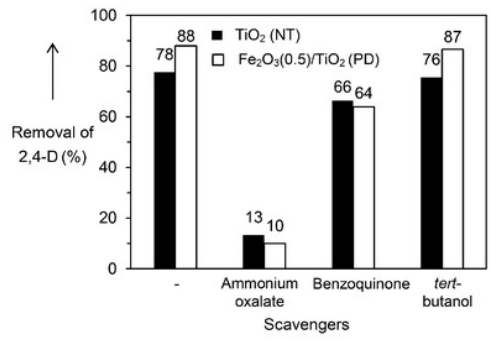


**Figure 7:** Percentage removal of 2,4-D on unmodified $TiO_2$ (NT) and $Fe_2O_3$($TiO_2$ (PD) in the absence and presence of various scavengers under UV light irradiation for 1 h.

Since the photogenerated holes on the $TiO_2$ have strong oxidizing power among oxidizing species [41], it is reasonable that holes are the most dominate active species in the oxidation of 2,4-D. Moreover, it has been reported that the oxidation of 2,4-D via a direct holes mechanism was favored at pH 3 [27]. In this study, an initial pH for 2,4-D was confirmed to be 3.2. On the other hand, superoxide radicals could be also easily formed for the oxidation reaction since the reaction was conducted in an open reactor, whereby the reduction of oxygen can easily take place. Related to the formation of hydroxyl radicals, it has been revealed that more hydroxyl radicals are formed from the adsorbed hydroxide ions with increased pH [28,42]. Therefore, it is likely that under the present conditions, they did not contribute as the active species probably due to their low formation.

The scavenger study was also conducted using the $Fe_2O_3(0.5)/TiO_2$ (PD) as shown in Figure 7. It was clear that the $Fe_2O_3(0.5)/TiO_2$ (PD) gave similar trend of activity as the ones obtained on the unmodified $TiO_2$ (NT). Both the photogenerated holes and superoxide radicals were important species, while hydroxyl radicals did not give much influence on the photocatalytic oxidation of 2,4-D. As compared to the unmodified $TiO_2$ (NT), the $Fe_2O_3(0.5)/TiO_2$ (PD) showed a more drastic reduction in the activity when the reactions were conducted in the presence of holes and superoxide radical scavengers. The activity decreased 8.8 and 1.4 times, respectively, as compared to those on $TiO_2$ (NT), i.e., 5.8 and 1.2 times, respectively. Such a result suggested the crucial role of $Fe_2O_3$ as a co-catalyst to improve the interfacial charge transfer and suppress electron–hole recombination. This leads to the formation of more photogenerated holes and superoxide radicals that contributed to an improved photocatalytic activity, as was also supported by the HRTEM, EIS and fluorescence spectroscopy results.

The stability of the $Fe_2O_3(0.5)/TiO_2$ (PD) sample was investigated by performing several cycles of photocatalytic reactions under UV light irradiation for 1 h. The $Fe_2O_3(0.5)/TiO_2$ (PD) sample gave a similar, comparable activity in a range of 82–88% even after 3 cycles of reactions, suggesting the good photostability of the $Fe_2O_3(0.5)/TiO_2$ (PD) nanocomposite and its potential application for photocatalytic water purification.

## Degradation and proposed mechanism

After the photocatalytic reactions on all samples, the formation of a 2,4-dichlorophenol (2,4-DCP) intermediate was observed

from the HPLC analysis, which was in good agreement with reported studies [15,28-32]. The 2,4-D degradation was then determined by Equation 2:

$$\text{2,4-D degradation}(\%) = \frac{[\text{2,4-D}]_I - [\text{2,4-D}]_F - [\text{2,4-DCP}]}{[\text{2,4-D}]_I} \times 100\% \quad (2)$$

where $[2,4\text{-D}]_I$ represents the initial concentration of 2,4-D after reaching adsorption–desorption equilibrium under dark conditions, $[2,4\text{-D}]_F$ is the final concentration of 2,4-D after lamp exposure and [2,4-DCP] is the concentration of the formed 2,4-DCP intermediate after lamp exposure. The percentage of 2,4-D degradation on the unmodified $TiO_2$ and the $Fe_2O_3/TiO_2$ (PD) series is given in Figure 8. Unmodified $TiO_2$ (NT) and $TiO_2$ (PD_T) showed a comparable degradation of 2,4-D of 6 and 5%, respectively. The addition of $Fe_2O_3$ was demonstrated to improve the photocatalytic activity of $TiO_2$ for degradation of 2,4-D. The $Fe_2O_3(0.5)/TiO_2$(PD) showed a 2,4-D degradation of 18%, which was three times higher than the unmodified $TiO_2$ (NT). Such enhanced performance was only slightly higher than that reported when using a Fe(III) nitrate nonahydrate precursor, which gave more than two times higher activity than the bare $TiO_2$ [15].

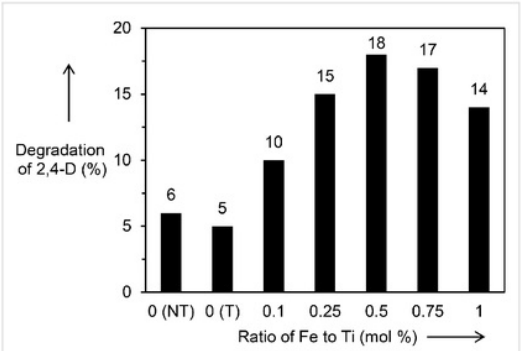


**Figure 8:** Photocatalytic degradation of 2,4-D on $TiO_2$ (NT), $TiO_2$ (PD_T) and the series of $Fe_2O_3/TiO_2$(PD) samples. NT represents no treatment, PD shows the samples were prepared by photodeposition method, and T indicates an additional photodeposition treatment was carried out on the sample.

The photocatalytic oxidation of 2,4-D by active species involves various steps, including formation of intermediates before its mineralization to $CO_2$ and $H_2O$. Decarboxylation has been reported as the initial step during the photocatalytic oxidation of 2,4-D when it is carried out at pH 3 [27]. The benzene ring opening and hydrocarbon chain breaking then took place, which finally led to the formation of $CO_2$ [29]. Since 2,4-DCP was detected as the dominant intermediate after the photocatalytic reactions, it could be suggested that 2,4-D was firstly oxidized by the active species (photogenerated holes and superoxide radicals) before decarboxylation and the formation of 2,4-DCP. The dechlorination of 2,4-DCP then took place, leading to ring opening, hydrocarbon chain breaking, and finally, the mineralization to $CO_2$ and $H_2O$ (see Supporting Information File 1, Figure S7).

The mechanism of major charge transfer pathways on the $Fe_2O_3(0.5)/TiO_2$ (PD) was also proposed and shown in Figure 9. When the photocatalyst is exposed to UV light, photo-

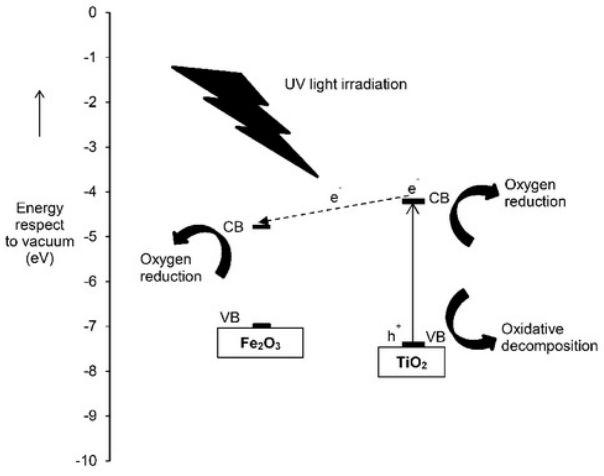


**Figure 9:** Proposed mechanism for major charge transfer pathways on $Fe_2O_3(0.5)/TiO_2$ (PD) for degradation of 2,4-D.

generated electrons are excited from the VB to the CB of $TiO_2$, while photogenerated holes are left in the VB. The photogenerated electrons could reduce oxygen to form superoxide radicals, while holes could directly oxidize 2,4-D to 2,4-DCP before its mineralization. The presence of $Fe_2O_3$ reduces electron–hole recombination on the $TiO_2$. Since the CB edge energy level of $Fe_2O_3$ (−4.78 eV relative to absolute vacuum scale (AVS)) is lower than that of $TiO_2$ (−4.21 eV relative to AVS) [43], $Fe_2O_3$ could act as an electron trapper that captured the photogenerated electrons from the $TiO_2$ that were not used for reduction of oxygen, instead of recombination with holes. Such electron transfer could suppress charge recombination on $TiO_2$ [5,10,12,14,15], whereby the oxidation of 2,4-D still could occur in the VB of $TiO_2$, and therefore, the photocatalytic degradation of 2,4-D could be improved. On the other hand, owing to the fast recombination of holes and electrons, the photocatalytic degradation of 2,4-D on bare $Fe_2O_3$ was negligible (1%). The oxidation of 2,4-D is unlikely to take place in the valence band of $Fe_2O_3$ and this would be the very minor pathway. Similar mechanisms have been also reported elsewhere [15].

## Conclusion

Two series of $Fe_2O_3/TiO_2$ nanocomposites were prepared by the impregnation and the photodeposition methods. The $Fe_2O_3/TiO_2$ nanocomposites prepared by the impregnation method showed less activity than the unmodified $TiO_2$ (NT), which was mainly due to the lower specific surface area caused by heat treatment. On the other hand, all the $Fe_2O_3/TiO_2$ nanocomposites prepared by the photodeposition methods exhibited superior photocatalytic activity as compared to the unmodified samples. The good photocatalytic activity of the nanocomposites was associated with the formation of a heterojunction between $Fe_2O_3$ and $TiO_2$ nanoparticles that promoted good charge transfer and suppressed electron–hole recombination. Scavenger studies showed that the photogenerated holes and superoxide radicals were the important active species in the reaction. The $Fe_2O_3(0.5)/TiO_2$ material showed excellent stability and reusability for the removal of 2,4-D. Among the nanocomposites, the $Fe_2O_3(0.5)/TiO_2$ sample showed the best activity, exhibiting 18% degradation of 2,4-D after 1 h of reaction, corresponding to three times higher activity compared to unmodified $TiO_2$.

## Experimental

### Materials

All chemicals and materials in the experiments were used without supplementary purification. The chemicals used were commercial Hombikat UV100 $TiO_2$ (UV100, Sachtleben Chemie), iron(III) acetylacetonate (99.9%, Sigma–Aldrich), ethanol (99.98%, HmbG® Chemicals), sodium sulfate (99.0%, Fisher Chemical), potassium ferricyanide (99.0%, Riedel-de Haën), 2,4-D (98.0%, Sigma), ammonium oxalate (99.5–101%, Merck), benzoquinone (99%, Acros Organics), and *tert*-butanol (99.0%, Merck).

### Sample preparation

The $TiO_2$ material used in this study was from the commercial supplier Hombikat, UV100 $TiO_2$. The $Fe_2O_3$ used as a control was prepared by direct calcination of Fe(III) acetylacetonate under air atmosphere at 500 °C for 4 h. Two series of $Fe_2O_3/TiO_2$ nanocomposites were prepared by impregnation and photodeposition methods. As for the synthesis of the nanocomposites via the impregnation method, an appropriate amount of Fe(III) acetylacetonate with varying mole percentage (mol %) of Fe/Ti of 0.1, 0.25, 0.5, 0.75 and 1 mol % were firstly dissolved in mixed solvents of water and ethanol (20 mL). Then, the commercial Hombikat UV100 $TiO_2$ (1 g) was dispersed in the Fe(III) acetylacetonate solution for 10 min by an ultrasonicator. The mixture was stirred and heated at 80 °C until all solvents were completely evaporated. The grind dried solid powder was then calcined at a temperature of 500 °C for 4 h. The prepared samples were labelled as $Fe_2O_3(x)/TiO_2$ (IM), where x relates to the loading of Fe/Ti in mol %. Bare $TiO_2$ with a similar heat treatment without the addition of the iron precursor was also prepared and denoted as $TiO_2$ (IM_T), while the $TiO_2$ without any pretreatment was denoted as $TiO_2$ (NT).

As for synthesis of the nanocomposites via the photodeposition method [20-22], an appropriate amount of Fe(III) acetylacetonate with various mole percentages of Fe/Ti (0.1, 0.25, 0.5, 0.75 and 1 mol %) were firstly dissolved in mixed solvents of water and ethanol (20 mL) by ultrasonication for few minutes. Then, the commercial Hombikat UV100 $TiO_2$ (1 g) was dispersed in the Fe(III) acetylacetonate solution by ultrasonic mixing for 10 min. The mixture was then stirred and irradiated under a 200 W Hg lamp (Hamamatsu, light intensity of 8 mW/cm² at 365 nm) at room temperature for 5 h. The solid was washed a few times with ethanol followed by deionized water before drying overnight inside an oven at 80 °C. Finally, the obtained solid powder was ground. The prepared samples were denoted as $Fe_2O_3(x)/TiO_2$ (PD), where x relates to the loading of Fe/Ti (in mol %). Bare $TiO_2$ undergoing a similar photodeposition treatment without the addition of the iron precursor was also produced and was denoted as $TiO_2$ (PD_T).

### Sample characterization

A Bruker D8 Advance diffractometer was used to measure the XRD patterns of the $TiO_2$ and the $Fe_2O_3/TiO_2$ samples prepared by both impregnation and photodeposition methods using a Cu Kα radiation source (λ = 0.15406 nm) at 40 kV and 40 mA. A Shimadzu UV-2600 DR UV–vis spectrophotometer was used to record the absorption spectra of samples, in which barium sulfate ($BaSO_4$) was used as a reference. The elemental

compositions (Fe, Ti) on the $Fe_2O_3/TiO_2$ (PD) nanocomposites were determined using an Agilent 700 series ICP-OES. The adsorption of nitrogen gas on the samples was measured at 77 K on a Quantachrome Novatouch LX4 instrument in order to determine the BET specific surface area of the samples.

TEM and HRTEM were performed on a JEOL JEM-2100 electron microscope with electron acceleration energy of 200 kV. EIS measurements were performed on a Gamry Interface 1000 potentiostat/galvanostat/ZRA. For the measurements of EIS, a screen printed electrode (SPE, DropSens) was used and prepared as follows. The photocatalyst sample (10 mg) was dispersed in water (6 mL) and the mixture was homogeneously mixed in an ultrasonic bath for 15 min. The mixture (20 µL) was then dropped onto the working electrode of the SPE, followed by immersion of the SPE in 6 mL of electrolyte which was a mixture of sodium sulfate (0.1 M) and potassium ferricyanide (2.5 mM). The frequency range was set in the range of 1 MHz to 100 mHz. A simplex model program (Gamry Echem Analyst) was selected to fit the obtained Nyquist plot by using constant phase element (CPE) with diffusion as the equivalent circuit model. The emission sites of the samples were investigated using a JASCO FP-8500 spectrofluorometer, in which the excitation wavelength was fixed at 218 nm. The reproducibility for emission spectra measurements was around 4%.

## Photocatalytic tests

The photocatalytic activity of the $Fe_2O_3/TiO_2$ nanocomposites prepared by both photodeposition and impregnation methods was tested for the removal of 2,4-D under irradiation of UV light for 1 h. The photocatalyst (50 mg) was dispersed in a 2,4-D solution (0.5 mM, 50 mL) and stirred for 1 h in the dark to achieve adsorption–desorption equilibrium. The photocatalytic reaction was then conducted under irradiation of a 200 W Hg-Xe lamp (Hamamatsu, light intensity of 8 mW/cm$^2$ at 365 nm) for 1 h at room temperature. After each reaction, the solution was separated from the photocatalyst by using a membrane filter. The concentration of 2,4-D was determined using a high-performance liquid chromatography instrument (Shimadzu, Prominence LC-20A with Hypersil gold PFP column), which was monitored at a wavelength of 283 nm. The percentage of 2,4-D removal was determined following Equation 3:

$$\text{2,4-D removal}(\%) = \frac{C_o - C_t}{C_o} \times 100\% \quad (3)$$

where $C_o$ is the initial concentration of 2,4-D after reaching adsorption–desorption equilibrium under dark conditions, while $C_t$ is the remaining concentration of 2,4-D after the reaction. Further investigation on the role of active species contributing to the removal of 2,4-D was carried out on the $Fe_2O_3(0.5)/TiO_2$ (PD) nanocomposite, which showed the best photocatalytic activity. Ammonium oxalate, benzoquinone, and *tert*-butanol were used as the various scavengers for photogenerated holes, superoxide radicals and hydroxyl radicals, respectively. The scavenger was introduced to the 2,4-D solution in the presence of the photocatalyst with 1 mole ratio of scavenger/pollutant.

The photostability of the $Fe_2O_3(0.5)/TiO_2$ (PD) nanocomposite was investigated by evaluating the photocatalytic activity for removal of 2,4-D over three cycles. After the first run of reaction under 1 h UV irradiation, the photocatalyst was collected from the 2,4-D solution and was washed with deionised water before drying at 80 °C overnight. The second and third cycles of reactions were conducted using the recovered photocatalyst under similar experimental and treatment conditions, as mentioned above.

## Supporting Information

### Supporting Information File 1

Additional figures.

The supporting information file contains seven figures with additional experimental data labelled as Figure S1–S7.

[http://www.beilstein-journals.org/bjnano/content/supplementary/2190-4286-8-93-S1.pdf]

## Acknowledgements

The research leading to these results has received funding from the European Union Seventh Framework Program (EU-FP7) under the 4G-PHOTOCAT grant (agreement no.: 309636). This work has been also financially supported by the Ministry of Higher Education (MOHE) and Universiti Teknologi Malaysia (UTM, Malaysia) through the international contract matching grant (cost center code: R.J130000.7626.4C035).

## References

1. Lazar, M. A.; Varghese, S.; Nair, S. S. *Catalysts* **2012,** *2,* 572–601. doi:10.3390/catal2040572
2. Gupta, M. S.; Triphati, M. *Chin. Sci. Bull.* **2011,** *56,* 1639–1657. doi:10.1007/s11434-011-4476-1
3. Ran, J.; Zhang, J.; Yu, J.; Jaroniec, M.; Qiao, S. Z. *Chem. Soc. Rev.* **2014,** *43,* 7787–7812. doi:10.1039/C3CS60425J
4. Yang, J.; Wang, D.; Han, H.; Li, C. *Acc. Chem. Res.* **2013,** *46,* 1900–1909. doi:10.1021/ar300227e
5. Sun, Q.; Leng, W.; Li, Z.; Xu, Y. *J. Hazard. Mater.* **2012,** *229–230,* 224–232. doi:10.1016/j.jhazmat.2012.05.098
6. Zhao, B.; Mele, G.; Pio, I.; Li, J.; Palmisano, L.; Vasapollo, G. *J. Hazard. Mater.* **2010,** *176,* 569–574. doi:10.1016/j.jhazmat.2009.11.066

7. Ghasemi, S.; Rahimnejad, S.; Setayesh, S. R.; Rohani, S.; Gholami, M. R. *J. Hazard. Mater.* **2009,** *172,* 1573–1578. doi:10.1016/j.jhazmat.2009.08.029
8. Shawabkeh, R. A.; Khashman, O. A.; Bisharat, G. I. *Int. J. Chem.* **2010,** *2,* 10–18. doi:10.5539/ijc.v2n2p10
9. Zhu, J.; Zheng, W.; He, B.; Zhang, J.; Anpo, M. *J. Mol. Catal. A: Chem.* **2004,** *216,* 35–43. doi:10.1016/j.molcata.2004.01.008
10. Xia, Y.; Yin, L. *Phys. Chem. Chem. Phys.* **2013,** *15,* 18627–18634. doi:10.1039/c3cp53178c
11. Li, X.; Lin, H.; Chen, X.; Niu, H.; Liu, J.; Zhang, T.; Qu, F. *Phys. Chem. Chem. Phys.* **2016,** *18,* 9176–9185. doi:10.1039/C5CP06681F
12. Barreca, D.; Carraro, G.; Warwick, M. E. A.; Kaunisto, K.; Gasparotto, A.; Gombac, V.; Sada, C.; Turner, S.; Van Tendeloo, G.; Maccato, C.; Fornasiero, P. *CrystEngComm* **2015,** *17,* 6219–6226. doi:10.1039/C5CE00883B
13. Balbuena, J.; Carraro, G.; Cruz, M.; Gasparotto, A.; Maccato, C.; Pastor, A.; Sada, C.; Barreca, D.; Sánchez, L. *RSC Adv.* **2016,** *6,* 74878–74885. doi:10.1039/C6RA15958C
14. Subramonian, W.; Wu, T. Y.; Chai, S.-P. *J. Environ. Manage.* **2017,** *187,* 298–310. doi:10.1016/j.jenvman.2016.10.024
15. Moniz, S. J. A.; Shevlin, S. A.; An, X.; Guo, Z.-X.; Tang, J. *Chem. – Eur. J.* **2014,** *20,* 15571–15579. doi:10.1002/chem.201403489
16. Litter, M. I.; Navío, J. A. *J. Photochem. Photobiol., A: Chem.* **1994,** *84,* 183–193. doi:10.1016/1010-6030(94)03858-9
17. Di Paola, A.; Marcì, G.; Palmisano, L.; Schiavello, M.; Uosaki, K.; Ikeda, S.; Ohtani, B. *J. Phys. Chem. B* **2002,** *106,* 637–645. doi:10.1021/jp013074l
18. Di Paola, A.; García-López, E.; Ikeda, S.; Marcì, G.; Ohtani, B.; Palmisano, L. *Catal. Today* **2002,** *75,* 87–93. doi:10.1016/S0920-5861(02)00048-2
19. Peña-Flores, J. I.; Palomec-Garfias, A. F.; Márquez-Beltrán, C.; Sánchez-Mora, E.; Gómez-Barojas, E.; Pérez-Rodríguez, F. *Nanoscale Res. Lett.* **2014,** *9,* No. 499. doi:10.1186/1556-276x-9-499
20. Siah, W. R.; Lintang, H. O.; Shamsuddin, M.; Yoshida, H.; Yuliati, L. *Catal. Sci. Technol.* **2016,** *6,* 5079–5087. doi:10.1039/C6CY00074F
21. Siah, W. R.; Lintang, H. O.; Yuliati, L. *Catal. Sci. Technol.* **2017,** *7,* 159–167. doi:10.1039/c6cy01991a
22. Roslan, N. A.; Lintang, H. O.; Yuliati, L. *Adv. Mater. Res.* **2015,** *1112,* 180–183. doi:10.4028/www.scientific.net/AMR.1112.180
23. Burns, C. J.; Swaen, G. M. H. *Crit. Rev. Toxicol.* **2012,** *42,* 768–786. doi:10.3109/10408444.2012.710576
24. El Harmoudi, H.; El Gaini, L.; Daoudi, E.; Rhazi, M.; Boughaleb, Y.; El Mhammedi, M. A.; Migalska-Zalas, A.; Bakasse, M. *Opt. Mater.* **2014,** *36,* 1471–1477. doi:10.1016/j.optmat.2014.03.040
25. Mustafa, Y. A.; Abdul-Hameed, H. M.; Razak, Z. A. *Clean: Soil, Air, Water* **2015,** *43,* 1241–1247. doi:10.1002/clen.201400623
26. Hu, J-y.; Morita, T.; Magara, Y.; Aizawa, T. *Water Res.* **2000,** *34,* 2215–2222. doi:10.1016/S0043-1354(99)00385-1
27. Sun, Y.; Pignatello, J. J. *Environ. Sci. Technol.* **1995,** *29,* 2065–2072. doi:10.1021/es00008a028
28. Djebbar, K.; Zertal, A.; Sehili, T. *Environ. Technol.* **2006,** *27,* 1191–1197. doi:10.1080/09593332708618732
29. Watanabe, N.; Horikoshi, S.; Suzuki, K.; Hidaka, H.; Serpone, N. *New J. Chem.* **2003,** *27,* 836–843. doi:10.1039/b211963n
30. Kim, J.; Choi, W. *Appl. Catal., B: Environ.* **2011,** *106,* 39–45.
31. Siah, W. R.; Lintang, H. O.; Shamsuddin, M.; Yuliati, L. *IOP Conf. Ser.: Mater. Sci. Eng.* **2016,** *107,* 012005. doi:10.1088/1757-899x/107/1/012005
32. Yuliati, L.; Siah, W. R.; Roslan, N. A.; Shamsuddin, M.; Lintang, H. O. *Malaysian J. Anal. Sci.* **2016,** *20,* 171–178. doi:10.17576/mjas-2016-2001-18
33. Pendlebury, S. R.; Wang, X.; Le Formal, F.; Cornuz, M.; Kafizas, A.; Tilley, S. D.; Grätzel, M.; Durrant, J. R. *J. Am. Chem. Soc.* **2014,** *136,* 9854–9857. doi:10.1021/ja504473e
34. Valencia, S.; Marín, J. M.; Restrepo, G. *Open Mater. Sci. J.* **2009,** *4,* 9–14. doi:10.2174/1874088x01004010009
35. Tian, G.; Fu, H.; Jing, L.; Xin, B.; Pan, K. *J. Phys. Chem. C* **2008,** *112,* 3083–3089. doi:10.1021/jp710283p
36. Devi, L. G.; Murthy, B. N.; Kumar, S. G. *Mater. Sci. Eng., B* **2010,** *166,* 1–6. doi:10.1016/j.mseb.2009.09.008
37. Khan, M. M.; Ansari, S. A.; Pradhan, D.; Ansari, M. O.; Han, D. H.; Lee, J.; Cho, M. H. *J. Mater. Chem. A* **2014,** *2,* 637–644. doi:10.1039/C3TA14052K
38. Nkosi, D.; Pillay, J.; Ozoemena, K. I.; Nouneh, K.; Oyama, M. *Phys. Chem. Chem. Phys.* **2010,** *12,* 604–613. doi:10.1039/B918754E
39. Cong, Y.; Zhang, J.; Chen, F.; Anpo, M. *J. Phys. Chem. C* **2007,** *111,* 6976–6982. doi:10.1021/jp0685030
40. Yang, M.-Q.; Zhang, Y.; Zhang, N.; Tang, Z.-R.; Xu, Y.-J. *Sci. Rep.* **2013,** *3,* 3314. doi:10.1038/srep03314
41. Munter, R. *Proc. Est. Acad. Sci., Chem.* **2001,** *50,* 59–80.
42. Trillas, M.; Peral, J.; Domènech, X. *Appl. Catal., B: Environ.* **1993,** *3,* 45–53. doi:10.1016/0926-3373(93)80067-N
43. Xu, Y.; Schoonen, M. A. A. *Am. Mineral.* **2000,** *85,* 543–556. doi:10.2138/am-2000-0416


## License and Terms